CLM-P755

CLM-P755

UKAEA

Preprint

ABSORPTION OF ELECTRON CYCLOTRON RADIATION IN TOKAMAK PLASMAS WITH A SUPERTHERMAL TAIL IN THE ELECTRON VELOCITY DISTRIBUTION

A. MONTES
R. O. DENDY

CULHAM LABORATORY
Abingdon Oxfordshire
1985

CLM-P 755

ABSORPTION OF ELECTRON CYCLOTRON RADIATION IN TOKAMAK PLASMAS WITH A SUPERTHERMAL TAIL IN THE ELECTRON VELOCITY DISTRIBUTION

A. Montes* and R. O. Dendy

Culham Laboratory, Abingdon, Oxon. OX14 3DB, U.K.

(Euratom/UKAEA Fusion Association)

Abstract

A monotonically decreasing superthermal tail in the distribution of electron velocities parallel to the tokamak magnetic field is represented by adding a drifted Maxwellian distribution to a bulk Maxwellian distribution. This combines a high degreee of flexibility in the set of tail parameters available with the possibility of obtaining exact analytic expressions for the dielectric tensor elements. Calculations have been carried out in the nonrelativistic limit, which restricts its applicability to the extraordinary mode away from normal incidence. A fully three-dimensional ray tracing code which includes the effects of toroidal geometry is employed. The results indicate that small tails (tail fraction $\simeq$ 0.5%) can significantly alter the wave absorption characteristics. These include the integrated absorption, spatial deposition profile, and velocity space deposition profile. Due to the presence of tail electrons, significant heating above the high density cutoff is found for high field side launching with $\omega = \Omega_e$(central), together with strong absorption at low density for low field side launching with $\omega << \Omega_e$(central).

(Submitted for publication in Physics of Fluids)

* Permanent address: Instituto de Pesquisas Espaciais, C.P.515, 12.200 - S.Jose dos Campos - S.P. - Brazil

August 1985

1. INTRODUCTION

Superthermal tails in the distribution of electron velocities parallel to the magnetic field have been observed both in Ohmically heated low density tokamak discharges[1] and in discharges supported by lower hybrid current drive.[2] Such tails have also been predicted to arise during current drive by electron cyclotron waves.[3] As shown in previous publications,[4-7] the tail is a very good absorber of electron cyclotron waves. In particular, for extraordinary mode absorption, which is the only case considered here, the physical reasons for the significance of the tail follow from the fact that absorption increases with the electron temperature.[8] The tail is a low-density, high-temperature component of the plasma which should accordingly be considered in the calculation of electron cyclotron resonance heating.

At any given time, the distribution in velocity space of the superthermal electrons in a specified region of real space is determined by a large number of effects. These include interparticle collisions, particle trapping, finite particle confinement time, forces arising from any externally applied field, interactions between electrons and plasma waves - both internally generated and externally applied - together with the nonlinear development of the instabilities to which extended tail distributions are subject. A number of interesting approaches have been made to this complex nonlinear problem;[3,7,9-12] however, no general solution exists at present. For this reason, previous authors have exercised some freedom in their choice of mathematical model for the tail when calculating its absorption characteristics.[4-7] These models include flat tails[4] and drifted Maxwellians in the weakly relativisitic limit;[5] a degree of self-consistency has also been included.[7] However, the

complexity of the calculations tends to restrict the range of parameters and the geometry which can be considered. In this paper, we have chosen to represent a monotonically decreasing tail by adding a nonrelativistic drifted Maxwellian distribution to a bulk Maxwellian distribution. The distributions considered here are consistent with typical values for the plasma current and with existing numerical simulations of tail formation; in addition, they give rise to a soft X-ray spectrum that is compatible with observations. Subject to these constraints, our model for the distribution function combines a high degree of flexibility in the set of tail parameters available with the possibility of obtaining exact analytic expressions for the dielectric tensor elements and their derived quantities. We can vary with ease the fraction of electrons in the tail, the mean tail velocity, and its thermal spread - and hence $\partial f/\partial v_{\parallel}$ - while the dielectric tensor elements can be expressed in terms of the standard plasma dispersion function. This relative simplicity allows us to use a fully three-dimensional ray tracing code.[13] We are able to trace a large number of rays, representing a realistic antenna pattern, in a realistic tokamak geometry for a wide range of plasma and tail parameters. In this frequency range, the ray tracing technique is a reliable method for computing the power deposition profile, both in real space and in velocity space, of the radiofrequency wave which is undergoing continuous refraction in the inhomogeneous medium. Ray tracing is particularly necessary in the high density regime, where refraction effects are extremely strong.

The nonrelativistic approach is valid so long as[14]

$$n_{\parallel} > \frac{v_e}{c} \qquad (1.1a)$$

$$n_{\parallel}^2 > \left|\frac{\omega - \Omega_e}{\omega}\right| \qquad (1.1b)$$

where $n_{\parallel}$ is the component of the refractive index parallel to the magnetic field, v_e is the electron thermal velocity, Ω_e is the electron cyclotron frequency - which we take to be positive - and ω is the frequency of the incident electromagnetic wave. We are therefore unable to deal accurately with propagation in directions close to perpendicular to the magnetic field direction, which is a regime in which absorption of the ordinary mode is much stronger than that of the extraordinary mode. Accordingly, we restrict ourselves to the case of X-mode propagation away from the perpendicular. This restriction is the price which must be paid for the relative simplicity of the analytical expressions employed.

2. Derivation of the Basic Equations

We consider an electron distribution function of the form

$$f(v_\perp, v_\parallel) = (1 - \mu) f_B(v_\perp, v_\parallel) + \mu f_T(v_\perp, v_\parallel) \qquad (2.1a)$$

$$f_B(v_\perp, v_\parallel) = \frac{\pi^{-3/2}}{v_{B\perp}^2 \, v_{B\parallel}} e^{-v_\perp^2/v_{B\perp}^2} e^{-v_\parallel^2/v_{B\parallel}^2} \qquad (2.1b)$$

$$f_\perp(v_\perp, v_\parallel) = \frac{\pi^{-3/2}}{v_{T\perp}^2 \, v_{T\perp}} e^{-v_\perp^2/v_{T\perp}^2} e^{-(v_\parallel - v_o)^2/v_{T\parallel}^2} \qquad (2.1c)$$

The small tail fraction μ, the drift velocity v_o, and the parallel thermal velocity $v_{T\parallel}$ characterising the drifted component are all chosen so that $f(v_\perp, v_\parallel)$ represents a distribution with a monotonically decreasing

superthermal tail, subject also to the constraints outlined in the Introduction; see, for example, Fig.1. In order to minimise the number of free parameters, we set $v_{B\perp} = v_{B\parallel} = v_B$ and $v_{T\perp} = v_{T\parallel} = v_T$ in Eqs. (2.1b,c), so that $f_B(v_\perp, v_\parallel)$ and $f_T(v_\parallel, v_\parallel)$ have no temperature anisotropy. The plasma is characterised by a plasma frequency ω_p, and the electric field amplitude $\underline{E}$ associated with the radiofrequency wave oscillates as $\exp[i\,\underline{k}.\underline{r} - i\omega t]$. We define

$$X = \left(\frac{\omega_p}{\omega}\right)^2, \quad Y = \left(\frac{\Omega_e}{\omega}\right) \tag{2.2a,b}$$

Wave propagation is determined by Maxwell's equations, which take the general form

$$\frac{c^2}{\omega^2}\,\underline{k} \times (\underline{k} \times \underline{E}) + \underline{\underline{\varepsilon}} \cdot \underline{E} = 0 \tag{2.3}$$

Substituting the electron distribution function, Eqs.(2.1a-c), into the standard general expression for the dielectric tensor $\underline{\underline{\varepsilon}}$,[15] we obtain

$$\varepsilon_{ij} = \begin{bmatrix} a_1 + W_{xx} & i(a_2 - W_{xx}) & W_{xz} \\ -i(a_2 - W_{xx}) & a_1 + W_{xx} & iW_{xz} \\ W_{xz} & -iW_{xz} & \varepsilon_3 + W_{zz} \end{bmatrix} \tag{2.4}$$

where

$$a_1 = 1 - \frac{X}{2(1+Y)} \; ; \quad a_2 = \frac{-X}{2(1+Y)} \; ; \quad \varepsilon_3 = 1 - X \tag{2.5a}$$

$$W_{ij} = W^B_{ij} + \mu W^T_{ij} \tag{2.5b}$$

$$W^B_{xx} = \frac{X}{2(1-Y)}\, \zeta Z(\zeta) \tag{2.5c}$$

$$W^T_{xx} = \frac{X}{2(1-Y')}\, \eta Z(\eta) \tag{2.5d}$$

$$W^B_{xz} = \frac{1}{2}\frac{n_\perp}{n_\parallel}\frac{X}{Y}\left[1 + \zeta Z(\zeta)\right] \tag{2.5e}$$

$$W^T_{xz} = \frac{1}{2}\frac{n_\perp}{n_\parallel}\frac{X}{Y}\left[1 + \eta\left(\frac{1-Y}{1-Y'}\right)Z(\eta)\right] \tag{2.5f}$$

$$W^B_{zz} = \frac{1}{2}\frac{n_\perp}{n_\parallel^2}\frac{X(1-Y)}{Y^2}\left[1 + \zeta Z(\zeta)\right] \tag{2.5g}$$

$$W^T_{zz} = \frac{1}{2}\frac{n_\perp^2}{n_\parallel^2}\frac{X(1-Y)}{Y^2}\left[1 + \eta\left(\frac{1-Y}{1-Y'}\right)Z(\eta)\right] \tag{2.5h}$$

$$Y' = \frac{\Omega_e}{\omega - k_\parallel v_o} \tag{2.5i}$$

Here X and Y are given by Eqs.(2.5a,b) and $n_\perp$ and $n_\parallel$ are the components of the refractive index $\underline{n} = c\underline{k}/\omega$ perpendicular and parallel to the magnetic

field direction. The standard plasma dispersion function[16] is represented by Z, and the arguments ζ and η are given by

$$\zeta = \frac{\omega - \Omega_e}{k_\parallel v_B} , \qquad \eta = \frac{\omega - k_\parallel v_o - \Omega_e}{k_\parallel v_T} \tag{2.6a,b}$$

We are concerned with waves in the electron cyclotron range of frequencies, $\omega \simeq \Omega_e$. Thus ζ and η will pass through zero at the warm plasma wave-particle cyclotron resonances arising in the bulk plasma and the tail component respectively.

We now combine Eqs.(2.3) and (2.5a-i) to obtain an expression which can be written in the form

$$D^C + D^W = 0 \tag{2.7}$$

Here the cold-plasma contribution D^C is given by the standard cold-plasma dispersion relation for electromagnetic waves:

$$D^C = (1 - Y^2)\{\varepsilon_1 n_\perp^4 + [(\varepsilon_1 + \varepsilon_3)n_\parallel^2 - \varepsilon_1\varepsilon_3 - (\varepsilon_1^2 - \varepsilon_2^2)]n_\perp^2 + \varepsilon_3 n_\parallel^4 - 2\varepsilon_1\varepsilon_3 n_\parallel^2 + \varepsilon_3(\varepsilon_1^2 - \varepsilon_2^2)\} \tag{2.8}$$

where ε_3 is given by Eq.(2.5a) and as usual

$$\varepsilon_1 = 1 - \frac{X}{1 - Y^2} , \qquad \varepsilon_2 = \frac{XY}{1 - Y^2} \tag{2.9a,b}$$

It follows from Eq.(2.7) that the imaginary part n_i of the refractive index is given by

$$n_i = \frac{-\mathrm{Im}\, D^w(n)}{\frac{n_\parallel}{n}\frac{\partial D^c}{\partial n_\parallel} + \frac{n_\perp}{n}\frac{\partial D^c}{\partial n_\perp}} \tag{2.10}$$

where $n_\perp$ and $n_\parallel$ satisfy $D^c(n_\perp, n_\parallel) = 0$. Writing $n_\perp = n\sin\theta$, $n_\parallel = n\cos\theta$, we have

$$\mathrm{Im}\, D^w = \frac{\pi^{1/2}\left|n_\parallel\right|(v_B/c)}{\left|Z(\zeta)\right|^2}(1 + Y)\left\{\Gamma_1(X,Y,n,\theta)e^{-\zeta^2} + \frac{2\mu}{(v_T n_\parallel/c)}\Gamma_2(X,Y,n,\theta)\left[F(\zeta)e^{-\eta^2} - F(\eta)e^{-\zeta^2}\right]\right\} \tag{2.11a}$$

where

$$\Gamma_1(X,Y,n,\theta) = D_1 + D_2 \tag{2.11b}$$

$$\Gamma_2(X,Y,n,\theta) = \frac{X}{2}D_o + (1 - Y)D_2 \tag{2.11c}$$

$$F(x) = e^{-x^2}\int_o^x e^{t^2}dt \tag{2.11d}$$

is the Dawson integral, ζ and η are given by Eqs.(2.6a,b), and D_0, D_1, and D_2 are given in the Appendix.

Equations (2.7)-(2.11) are the basis for our ray tracing study of the propagation and absorption of electromagnetic waves in the electron cyclotron range of frequencies when the electron velocity distribution has an energetic tail. We note for completeness that in the absence of a tail (μ=0), these equations reduce to those of Akhiezer et al.[17]

3. NUMERICAL RESULTS

The ray tracing code[13] has been modified to include the imaginary part of the refractive index, derived in the previous section, and is used to calculate the power deposition along the ray path.

Ray tracing, or the geometrical optics approximation, is discussed in a number of texts, see for example Refs.14,18,19. Provided that the scale-lengths associated with plasma inhomogeneity are much larger than typical wavelengths and that dissipative effects are weak, so that little attenuation occurs within a single wavelength, a group velocity can be defined which determines the trajectory followed by a wave packet. The rate at which the local properties of the wave change along this trajectory can be derived from the local cold plasma dispersion relation.[18] For a given plasma equilibrium configuration, the ray equations are

$$\frac{d\underline{r}}{dt} = \underline{v}_g = \frac{\partial u}{\partial \underline{k}} \tag{3.1a}$$

$$\frac{d\underline{k}}{dt} = - \frac{\partial u}{\partial \underline{r}} \tag{3.1b}$$

Here $\underline{r}$ is the position vector, relative to the centre of the plasma, of a point on the ray, and $\underline{k}$ is the local wavevector; and $u(\underline{k},\underline{r}) = \omega$ is the

cold plasma dispersion relation for the mode under consideration, which is externally excited with frequency ω. The power remaining in the ray after it has propagated a path length ℓ is

$$P(\ell) = P_o \, e^{-\tau(\ell)} \tag{3.2}$$

where

$$\tau(\ell) = 2\int_o^{\ell} \underline{k}_i \cdot d\underline{\ell} = \frac{2\omega}{c} \int_o^{\ell} n_i \, \underline{\underline{k}} \cdot d\underline{\ell} \tag{3.3}$$

is the optical depth.

The plasma equilibrium is represented by the following profiles for the electron density, the electron temperature, and the toroidal and poloidal magnetic fields:

$$n_e(r) = n_e(0) \left(1 - \frac{r^2}{a^2}\right)^{\alpha} \tag{3.4a}$$

$$T_e(r) = T_e(0) \left(1 - \frac{r^2}{a^2}\right)^{\beta} \tag{3.4b}$$

$$B_T(\underline{r}) = B_T(0)/\left(1 + \frac{x}{R_o}\right) \tag{3.4c}$$

$$B_p(r) = B_p(a)\frac{a}{r}\left[1 - \left(1 - \frac{r^2}{a^2}\right)^{1 + \frac{3\beta}{2}}\right] \tag{3.4d}$$

where $r^2 = x^2 + y^2$ and a and R_o are the plasma minor and major radius, respectively. The total magnetic field is given by

$$\underline{B}(\underline{r}) = B_T(\underline{r})\hat{\underline{e}}_z + \underline{B}_p(r) \tag{3.5}$$

In our ray-tracing calculations, the parameters are chosen to represent the DITE tokamak: $R_o = 1.17$m, $a = 0.26$m, and $\alpha = \beta = 1$. Unless otherwise stated, the toroidal magnetic field intensity is determined by assuming $\omega = \Omega_e(0)$, so that for an electromagnetic wave with $\omega = 60$ GHz, we have $B_T(0) = 2.14$ T. The central electron temperature is kept constant,
$T_e(0) = 1.5$ keV. The central electron density is varied from $n_e(0) = 2 \times 10^{19}$ m^{-3} to 1.4×10^{20} m^{-3}; we note that for $n_e(0) > 8 \times 10^{19}$ m^{-3} the X-mode high-density cutoff is present in the plasma.

The rays are launched from the plasma edge with initial wavevector $\underline{k}_0$ (the vacuum wavenumber $k_0 = \omega/c$) which are given a conical distribution in order to represent a typical antenna pattern. In all cases, the full cone angular aperture was taken to be 10°. As mentioned in Section 1, our analysis is carried out only in the nonrelativistic limit. It follows that the analysis is not appropriate for launch angles close to the perpendicular, see Eqs.(1.1a,b). For this reason, we have not dealt with O-mode absorption, which is known to be greatest for launch angles near the perpendicular.[14] We have restricted our treatment to the X-mode, whose absorption increases from zero as the launch angle moves away from the perpendicular.[14] To simulate typical experimental arrangements, we have in most cases chosen a launch angle of 120°, for which our nonrelativistic analysis remains valid.

The parameters μ, v_o, and T_T characterise the deviation of the

electron velocity distribution from a single bulk Maxwellian. The identification of these mathematically convenient parameters with physical properties of the tail is to some extent dependent on the definition of the tail. It should be noted that if we define the tail as consisting of all those electrons with parallel velocities exceeding some value v_*, the number of tail electrons will depend on all three parameters. Thus, as T_T is increased at constant μ and v_o, a greater proportion of the electrons in the drifted Maxwellian acquire parallel velocities below v_*. This reduces the number of electrons in the tail at the same time as the high-velocity end of the drifted Maxwellian distribution, penetrating to higher values of $v_\parallel$, extends the range of the tail. On the other hand, the fraction of electrons in the tail is proportional to μ at constant v_o and T_T. We have therefore chosen to discuss tail absorption in terms of the parameters μ, v_o and T_T, and draw attention to the effects outlined above as they occur. The range of parameter values considered has been chosen to be consistent with the results of numerical simulations of tail formation.[7,20] In addition, there are two further constraints. Firstly, we consider only tails that are monotonically decreasing. Secondly, the asymmetry in the parallel velocity distribution arising from the tail is responsible for the current, and the current must take values which are reasonable for the tokamak plasma considered. Subject to these constraints, we have attempted to sample a wide range of tail formations. Typical values are $\mu = 0.005$, $v_o = 3v_B$, and $T_T = 13.5$ keV; this corresponds to a plasma current of $I_p \simeq 200$ kA when $n_e(0) = 4 \times 10^{19} m^{-3}$. The corresponding $v_\perp = 0$ cross section of the velocity distribution function is shown in Fig. 1.

3.1 LOW DENSITY CASE

For $n_e(0) < 8 \times 10^{19}$ m^{-3}, the X-mode has no cutoff in the plasma, and the electron cyclotron resonance is accessible to the radiation. This case is similar to that investigated by Fidone and co-workers[5] in slab geometry.

Minor cross section projections of the three-dimensional ray trajectories are shown in Fig. 2a (tail parameters $\mu = 0.005$, $v_o = 3.0\ v_e$, $T_T = 13.5$ keV). It can be seen that in the presence of a tail, a significant fraction of the absorption takes place well away from the electron cyclotron resonance $\omega = \Omega_e(x)$. This is due to the down-shifted resonance with the high-$v_\parallel$ electrons in the tail, $\omega = \Omega_e + k_\parallel v_\parallel$, with $k_\parallel < 0$ since we have a launch angle of 120°. The associated radial and velocity space power deposition profiles are shown in Fig. 2b and Fig. 2c. In both cases the effect of the tail can be seen in the substantial increase in absorption at large radius (high $v_\parallel$) and corresponding decrease in absorption at small radius (small $v_\parallel$). The resonance condition relates $v_\parallel$ to position : $v_\parallel = \left(\omega - \Omega_e(x)\right)/k_\parallel$. In the high temperature bulk plasma considered here, absorption is so effective that power deposition exceeding 90% is achieved before the rays reach the resonance $\omega = \Omega_e(x)$. In Fig. 2d, the quantity $\sum P(v_\parallel)$ denotes the power absorbed by electrons having parallel velocity above $v_\parallel$, as a percentage of the total power absorbed. With no tail, absorption for $v_\parallel \geq 3.0\ v_B$ is negligible. In the presence of a small tail, approximately 35% of the absorption occurs in this high velocity domain.

We now examine in detail how the absorption as a function of $v_\parallel/v_B$ varies with the tail parameters and launch angle. It should be stressed that $v_\parallel/v_B$ can be mapped to the x-coordinate through the nonrelativistic resonance condition. In particular, $v_\parallel/v_B = 0$ corresponds to the position of the fundamental cyclotron resonance $\left(\omega = \Omega_e(x)\right)$, while $v_\parallel/v_B = +\infty$ $(-\infty)$

corresponds to the high field side plasma edge for a launch angle larger (smaller) than 90°.

In Fig. 3 the parameter varied is the fraction μ of electrons in the drifted Maxwellian. For values of μ as low as 10^{-3}, approximately 10% of the incident power is absorbed in the tail, while for $\mu = 10^{-2}$ the tail absorption rises to 60%. It is interesting to note that for $\mu = 5 \times 10^{-2}$, almost 100% of the incident power is absorbed by the tail.

The fraction of electrons with parallel velocity exceeding a value v_* is given by

$$\mu_T = \frac{1}{2}\left\{(1-\mu)\,\mathrm{cerf}(u_*) + \mu\left[1 \pm \mathrm{erf}\left(\pm \frac{\beta_o - u_*}{\beta_T}\right)\right]\right\}, \quad u_* \lesssim \beta_o \qquad (3.6)$$

where $u_* = v_*/v_B$, $\beta_o = v_o/v_B$, $\beta_T = v_T/v_B$, erf(x) is the error function and cerf(x) = 1 - erf(x) is the complementary error function.

It follows that when we vary v_o or T_T while keeping other variables constant, a number of factors influence absorption by the tail. In Fig. 4, the drift velocity v_o is varied at constant (μ, T_T), subject to the constraint that the tail is monotonically decreasing. As v_o is increased, (i) μ_T increases, (ii) a plateau region begins to form, reducing the mean value of $\partial f/\partial v_\parallel$, (iii) the Doppler-shifted cyclotron resonance moves towards the edge of the plasma, where density and temperature are both lower, and (iv) the number of electrons at high $v_\parallel$ increases. These effects combine to produce the steady increase of tail absorption with v_o shown in Fig. 4. In Fig. 5, the thermal spread of velocities in the tail is varied at constant (μ, v_o). As v_T/v_B is increased, the number of electrons at high values of $v_\parallel$ increases, μ_T decreases, and the gradient of the velocity distribution function in the parallel direction decreases. It can be seen that absorption by the tail occurs at larger $v_\parallel$ for higher

values of v_T/v_B. However, integrated absorption by the tail decreases as v_T/v_B increases; this is due to the associated decrease in the value of μ_T and of the mean velocity gradient.

We note that in general, as the launch angle increases from 90°, so does the right circularly polarised component. The wave is therefore absorbed more efficiently by the electrons. Since the wave interacts first with the tail electrons, these absorb an increasing proportion of the incident power. The effect of reversing the orientation of the wave vector with respect to the toroidal magnetic field direction is shown in Fig. 6. Since at resonance $v_{\parallel} = (\omega - \Omega_e)/k_{\parallel}$, for $k_{\parallel} > 0$ the tail electrons interact with the wave only on the low field side of the resonance $\omega = \Omega_e(x)$. However, the wave is incident from the high field side; It has therefore undergone strong attenuation by the bulk electron distribution before it reaches the tail electrons. Conversely, for $k_{\parallel} < 0$ the wave interacts first with the tail electrons. The residual absorption by the tail electrons for $k_{\parallel} > 0$ can be compared to the stronger absorption for $k_{\parallel} < 0$.

3.2 HIGH DENSITY CASE

For $n_e(o) > 8 \times 10^{19}$ m^{-3}, the X-mode has a high-density cutoff, so that the rays are strongly refracted away from the centre of the plasma. The electron cyclotron resonance of the bulk thermal electron distribution is therefore inaccessible to the waves. However, some tail electrons may be sufficiently energetic for their Doppler-shifted electron cyclotron resonance to lie in the outer region of the plasma which is crossed by the waves before they are refracted away from the high-density cutoff. It is clear that the employment of ray-tracing techniques is indispensable.

The results of calculations in this regime for typical tail parameters ($\mu = 5 \times 10^{-3}$, $v_o/v_B = 4.5$, $T_T = 13.5$ keV) are shown in Figs. 7a-c. For the bulk plasma parameters shown in Fig. 7a, power deposition is localised to the edge of the plasma and is due exclusively to tail electrons, see Fig. 7b. Significant integrated absorption ≃ 38% occurs even for this small tail (Fig. 8c). It should be noted that in this high-density regime, the plasma current associated with given values of (μ, v_o, T_T) is proportionately greater than in the low-density case; typical values lie close to 1 MA.

The dependence of absorption on a range of parameters is shown in Figs. 8-10. In Figs. 8 and 9, the parameters μ and v_o are varied. The absorption has only weak dependence on T_T. It should be added as the plasma density increases, the X-mode cutoff moves outwards, shielding the position of the Doppler-shifted cyclotron resonance for electrons of increasingly high $v_\parallel$. The possibility of wave-particle resonance is therefore increasingly confined to the high-energy tail of the distribution, where the number of electrons falls steadily. In Fig. 10, the increase in tail absorption with angle of incidence is shown. This increase is due to two factors. As $|k_\parallel|$ increases, the resonance moves outwards into a region of increased wave energy; at the same time, the wave remains within the resonance region for a longer period.

These results show that significant power deposition can occur for high-density plasmas in which the X-mode cutoff is present, provided that the electron velocity distribution has a superthermal tail with $\mu \geq 5 \times 10^{-3}$. This suggests that the presence of a small tail should be examined as a possible explanation for the recent experimental results on Doublet-III[21] and FT-1[22], where significant absorption was observed for densities above the X-mode cutoff. In addition, we note that in this

regime the wave energy is deposited exclusively among the high-$v_{\parallel}$ tail electrons, which are the most efficient targets for current drive.

3.3 LOW FIELD SIDE LAUNCHING

In this Section we examine a heating and current drive scenario proposed by Fidone and co-workers.[4] Suppose that the gyrotron source has a frequency $\omega << \Omega_e(0)$, so that the resonance $\omega = \Omega_e(x)$ lies outside the torus. In this case, a launch position on the outside edge of the torus is located on the high-field side of the fundamental cyclotron resonance. The resonance condition $v_{\parallel} = (\omega - \Omega_e)/k_{\parallel}$ shows that only high-$v_{\parallel}$ electrons will interact with the wave. Heating is therefore confined to any superthermal tail electrons that may be present, and this would be particularly effective in current drive. This method is additionally attractive for engineering reasons. Firstly, a lower-frequency gyrotron can be used than in the usual case where $\omega = \Omega_e(0)$; secondly, access is easier for a launch position on the outside of the torus.

The results of the ray-tracing calculations for a typical set of parameters ($\mu = 5 \times 10^{-3}$, $v_o/v_B = 3$, $T_T = 13.5$ keV) are shown in Figs. 11a-c. In Figs. 11a,b it can be seen that power is deposited uniformly around the centre of the plasma; this is probably advantageous in terms of plasma stability. The absorption profile in velocity space is strongly peaked (Fig. 11c), and the integrated power deposited for this small value of μ is 70%. Such large absorption by the tail can be explained in terms of the polarisation of the wave, which is propagating away from the fundamental cyclotron resonance on the high-field side. As the wave approaches the centre of the plasma, the right circularly polarised component is substantially greater than would be the case if the cyclotron resonance were located at the centre.

The variation of absorption with tail parameters is shown in Figs. 12-14. In this heating regime, unlike that discussed in Sections 3.1 and 3.2, $v_{\parallel}/v_B$ does not map uniquely to the spatial coordinate x. This problem arises because of the spatial variation in v_B, which tends to zero at the edge of the plasma. However, the graphs display clearly the total absorption in each case. The power deposition profile in velocity space is given by the derivative of the curves in Figs. 12-14, so that the width of the resonance region in velocity space can be seen. In Fig. 12, the variation of absorption with tail density μ is shown. As the tail density increases, so does the integrated absorption, while the resonance region in velocity space narrows. There is a large variation in the integrated absorption: for a very small tail, $\mu = 10^{-3}$, a figure of 20% is obtained, while 100% absorption occurs for $\mu = 5 \times 10^{-2}$. The effect of variations in v_o and T_T, which produce a number of changes in the characteristics of the tail as discussed in the preceding sections, are shown in Figs. 13 and 14 respectively. Both the integrated absorption and the width of the resonance region in velocity space increase with the tail drift velocity. An increase in the tail temperature has little effect on the integrated absorption, but causes a large increase in the width of the resonance region. In Fig. 15, the integrated absorption is seen to decrease as the bulk plasma density increases. This decrease is due to the diminution in the right circularly polarised component of the wave as ω_p increases. The integrated absorption has been found to increase with the launch angle, as expected. For a tail characterised by $\mu = 5 \times 10^{-3}$, $v_o/v_B = 3$ and $T_T = 13.5$ keV, integrated absorption is 70% for $\theta = 120°$ and 98% for $\theta = 135°$.

4. CONCLUSIONS

We have represented a monotonically decreasing superthermal electron tail distribution by adding a drifted Maxwellian distribution, which is parametrised by suitable values of (μ, v_o, T_T), to a bulk Maxwellian distribution. The range of tail formations which can be described in terms of (μ, v_o, T_T) is very large, and it would be difficult to justify the use of further free parameters in a study of this kind. This representation gives rise to relatively simple analytic expressions for the absorption of waves in the electron cyclotron range of frequencies in the nonrelativistic regime, which have been used in conjunction with a ray tracing code to study X-mode absorption away from normal incidence. By varying the three basic parameters, the dependence of absorption on the nature of the tail distribution and on the launch angle has been quantified over a wide range of values. The results obtained include ray trajectories showing absorption along the ray, real space and velocity space deposition profiles, and integrated absorption profiles.

We conclude firstly that even small tails ($\mu = 5 \times 10^{-3}$, $v_o/v_B = 3$, $T_T = 13.5$ keV) can absorb a disproportionate fraction $\geq 30\%$ of the incident power at low density; this fraction exceeds 90% for $\mu = 5 \times 10^{-2}$. Secondly, we have shown that a similar small tail can absorb significant amounts of radiation in a high-density plasma in which the X-mode cutoff shields the cyclotron resonance of the bulk thermal electrons. Finally, we have considered the case of a low-frequency gyrotron, $\omega << \Omega_e(0)$, for which the cyclotron resonance lies outside the torus. In this case, a small tail alone can absorb upwards of 80% of the incident X-mode radiation which is launched from the outside of the torus; the absorption remains high for a wide range of parameter values. This arrangement appears well-suited to current drive, since the heating occurs

in a broad region around the centre of the plasma and is concentrated exclusively on tail electrons. It is additionally attractive due to engineering considerations. Firstly, a gyrotron with a frequency substantially lower than the central plasma cyclotron frequency can be employed; secondly, access is easier for a launch position on the outside of the torus.

The results presented in this paper deal with the essentially linear problem of the absorption of electron cyclotron waves by a given distribution with a superthermal tail. In the longer term, it will be necessary to address a general self-consistent nonlinear problem of the type outlined in the Introduction. It is known that the absorption of radiofrequency waves by a bulk thermal plasma can produce a tail; the waves will then interact further with the tail, and their absorption will in part determine the continued evolution of the tail.

We conclude by remarking that in general, small tails have a disproportionately large effect on the absorption of cyclotron waves, both in low-density and in high-density regimes. It is hoped that some of the information presented in this paper will give an indication of how anomalous absorption effects can be interpreted in terms of tail structure. Conversely, independent information on the presence and extent of a tail in the electron velocity distribution will be helpful in interpreting experimental absorption data.

ACKNOWLEDGEMENT

One of the authors (A.M.) wishes to thank the Conselho Nacional de Desenvolvimento Cientifico e Tecnologico (CNPq) - Brazil for partial financial support.

Appendix

The quantities D_o, D_1, and D_2 arising in Eqs.(2.11b,c) are given by

$$D_0 = \sin^2\theta\, n^4 - \left[2(1-2Y^2)\sin^2\theta + (1-X)\cos^2\theta\right]n^2 + 2(1-X)(1-2Y^2) \quad \text{(A.9a)}$$

$$D_1 = \left[(1-Y^2)\sin^2\theta + (1-X)\cos^2\theta\right]n^4$$

$$-\left[(1-Y^2)(1-X)(1+\cos^2\theta) + (1-2Y^2)\sin^2\theta\right]n^2 + (1-X)(1-2Y^2) \quad \text{(A.9b)}$$

$$D_2 = \frac{X}{Y}\sin^2\theta\, n^2(n^2-1+2Y^2) + \frac{1}{4}\frac{X}{Y^2}\frac{\sin^2\theta}{\cos^2\theta}\left[(1+\cos^2\theta)n^2 - 2(1-2Y^2)\right]$$

$$+ \frac{1}{2}\frac{X(1-Y)}{Y^2}\frac{\sin^2\theta}{\cos^2\theta}\left[\cos^2\theta\, n^4 - (1-Y^2)(1+\cos^2\theta)n^2 + (1-2Y^2)\right] \quad \text{(A.9c)}$$

REFERENCES

1
H. Knoepfel and D.A. Spong, Nucl. Fusion 9, 785 (1979).

2
S. Von Goeler, J. Stevens, C. Karney, and PLT Team, Fifth A.P.S. Topical Conf. on Radio Frequency Plasma Heating, Madison, Wisconsin (1983).

3
C.F. Karney and N.J. Fisch, Phys. Fluids 22, 1817 (1979).

4
I. Fidone, G. Giruzzi, A. Granata, and R.L. Meyer, Phys. Fluids 27, 661 (1984); I. Fidone, G. Giruzzi, and E. Mazzucato, Phys. Fluids 28, 1224 (1985)

5
I. Fidone, G. Granata and R.L. Meyer, Plasma Phys. 22, 261 (1980); M. Bornatici and U. Ruffina, Proc. Spring College on Plasma Physics, ICTP, Trieste, Italy (1985).

6
D. Farina, M. Lontano, and R. Pozzoli, Proc. 2nd Joint Varenna-Grenoble Int. Symp. on Heating in Toroidal Plasmas, Como, Italy (1980).

7
U. Krivenski, I. Fidone, G. Giruzzi, G. Granata, E. Mazzucato, and R.L. Meyer, Preprint EUR-CEA-FC-1236 (1984);
I. Fidone, A. Giruzzi, G. Granata, V. Krivenski, and R.L. Meyer, Preprint EUR-CEA-FC-1237 (1984);
A. Giruzzi, V. Krivenski, I. Fidone, and L.S. Ziebell, Preprint EUR-CEA-FC-1257 (1985);
D. Farina, M. Lontano, and R. Pozzoli, Proc. 4th Int. Workshop on ECE and ECRH, Frascati, Italy (1984).

8
M. Bornatici and F. Engelmann, Radio Sci. 14, 309 (1979).

9
J. Vaclavik, K. Appert, A.H. Kritz, and L. Muschietti, Plasma Phys. 25, 1283 (1983).

10
M.G. McCoy, A.A. Mirin, and J. Killeen, Comp. Phys. Comm. 24, 37 (1981); G.D. Kerbel and M.G. McCoy, Preprint UCRL-92062 (1984).

11
J.G. Cordey, T. Edlington, and D.F.H. Start, Plasma Phys. 24, 73 (1982).

12
C.S. Liu, Y.C. Mok, K. Papadopoulos, F. Engelmann, and M. Bornatici, Phys. Rev. Lett. 39, 701 (1977).

13
P. Fielding, private communication.

14
M. Bornatici, R. Cano, O. De Barbieri, and F. Engelmann, Nucl. Fusion 23, 1153 (1983).

15
N.A. Krall and A.W. Trivelpiece, Principles of Plasma Physics" (McGraw-Hill, London, 1973).

16
B.D. Fried and S.D. Conte, "The Plasma Dispersion Function" (Academic, New York 1961).

17
I. Akhiezer, I.A. Akhiezer, R.V. Polovin, A.G. Sitenko, and K.N. Stepanov, "Plasma Electrodynamics", Vol. I. (Pergamon, Oxford 1975).

18
I.B. Bernstein, Phys. Fluids 18, 320 (1975); H. Weitzner and D.B. Batchelor, Phys. Fluids 23, 1359 (1980).

19
K.G. Budden, "Radio Waves in the Ionosphere" (Cambridge U.P., Cambridge, 1961).

20
M. O'Brien, M. Cox, and D.F.H. Start, to be submitted to Plasma Phys.

21
R. Prater, S. Ejima, J.Y. Hsu, S.H. Lin, C. Moeller, R. Stockdale, Doublet-III Group and JAERI Group, Bull. Am. Phys. Soc. 29, 1427 (1984).

22
Yu.F. Baranov, D.G. Bulyginsky, V.E. Golant, V.I. Ivanov, M.M. Larionov, L.S. Levin, V.V. Rozhdestuensky, A.K. Salakhitdinov, A.I. Tokunov, V.I. Fedorov, and N.V. Shustova, Proc. 10th Eur. Conf. on Controlled Fusion and Plasma Physics, (Moscow, Paper H-8 (1981); D.A. Bulyginsky, V.E. Golant, S.G. Goncharov, V.K. Gusev, M.M. Larionov, L.S. Levin, G.T. Razdobarin, A.I. Smirnov, and N.V. Shustova, ibid., Supplement, page 171 (1981).

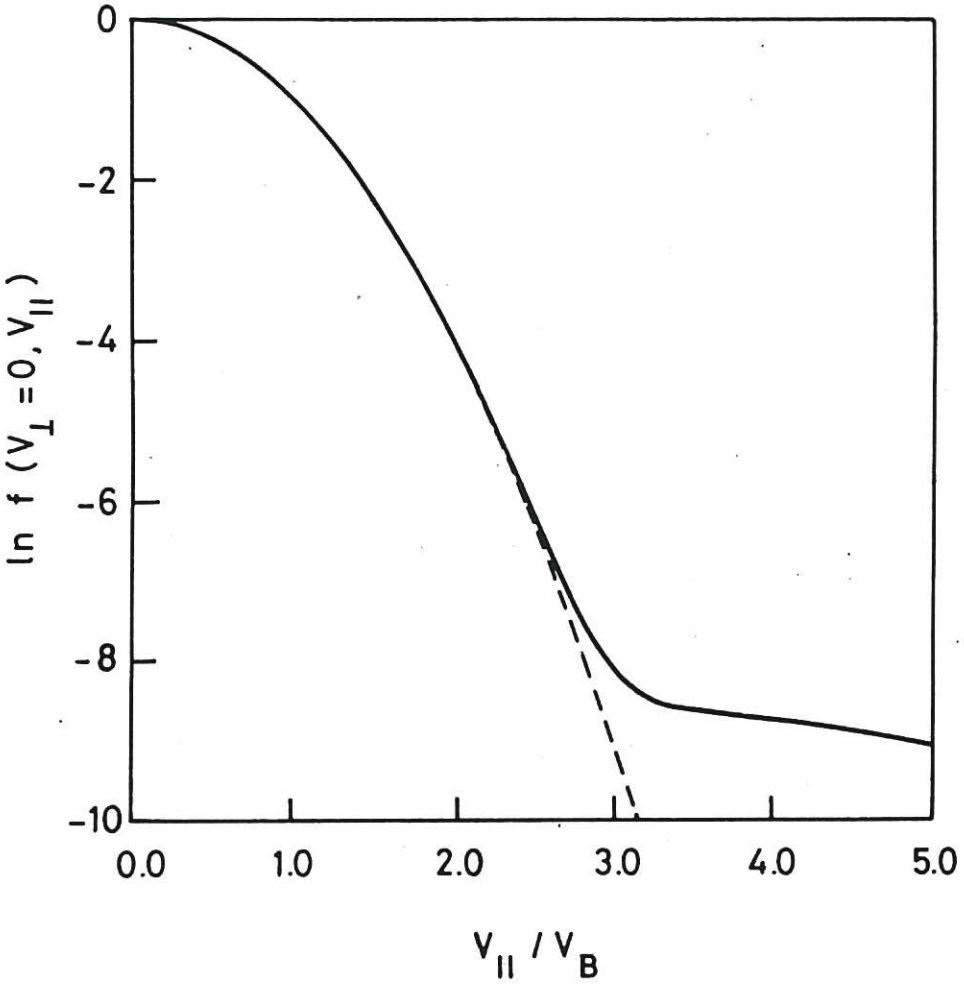

Fig. 1 Example of the velocity distribution function used in the calculations. The dashed line represents the bulk Maxwellian.

CLM-P755

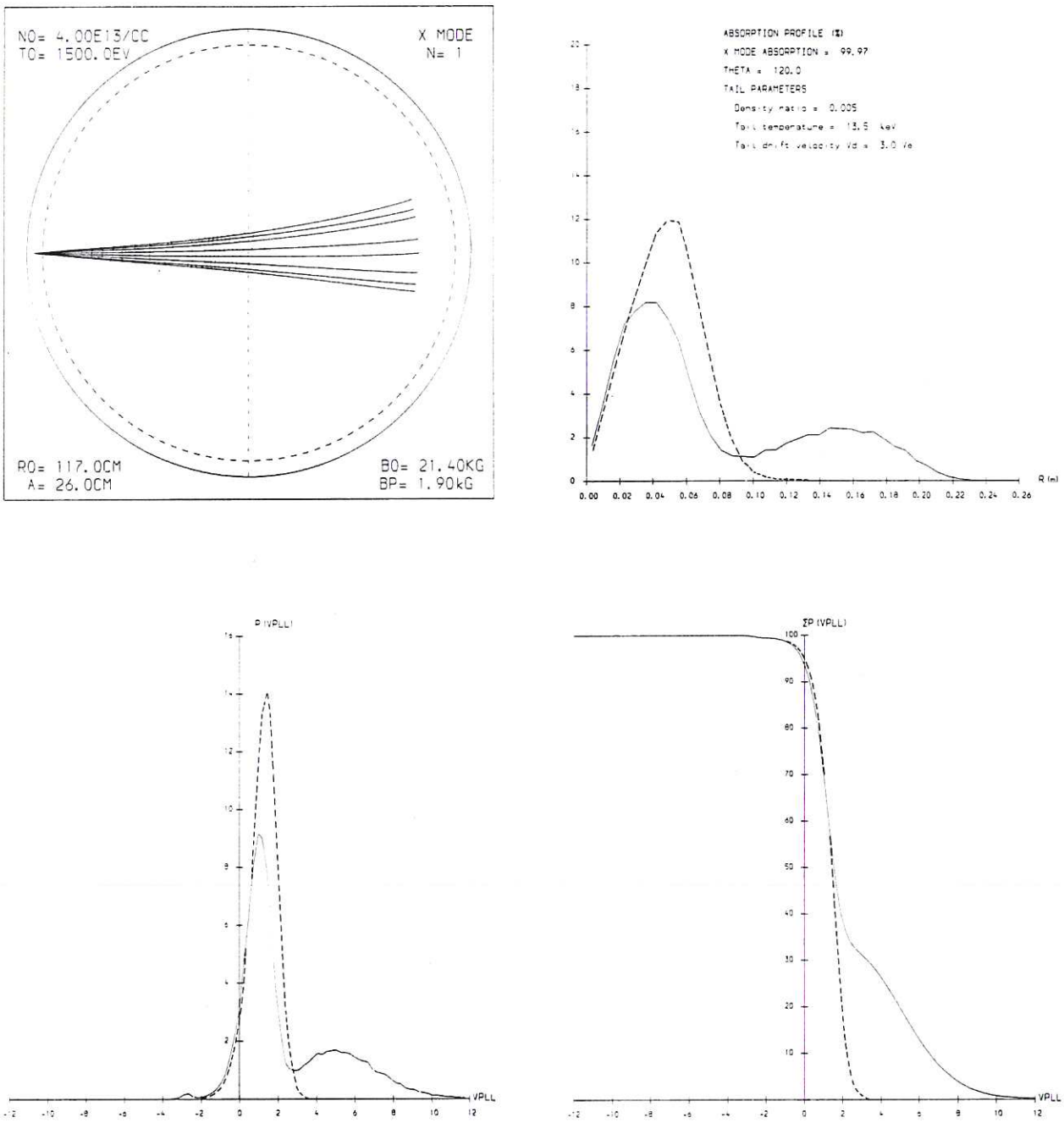

Fig. 2(a) Minor cross section projection of ray trajectories in the presence of a tail. The plasma parameters are displayed. Each cross on a ray marks a 5% decrease in the power carried by the ray. The vertical dashed line marks the position $\omega = \Omega_e(x)$. Rays terminate at the upper hybrid resonance. (b) Power deposited per unit radial coordinate interval and (c) per unit parallel velocity interval. The dashed curve shows the result in the absence of a tail. (d) Integrated power diposition. The rays are incident from the right, and are absorbed first by the high-$V_{\parallel}$ electrons. The dashed curve shows the result in the absence of a tail.

CLM-P755

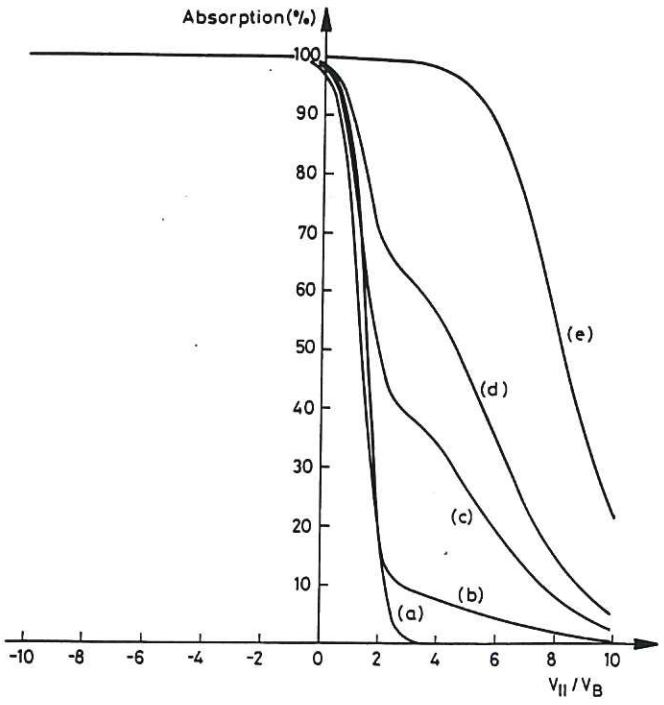

Fig. 3 Integrated power deposition profile. The rays are incident from the right. $n_e(0)=4\times10^{19}\,m^{-3}$, $T_e(0)=1.5\,keV$, launch angle 120°. Tail parameters: $v_0=3.0\,b_B$, $T_T=13.5\,keV$ and (a) $\mu=0.0$, (b) $\mu=0.001$, (c) $\mu=0.005$, (d) $\mu=0.01$, (e) $\mu=0.05$.

CLM-P755

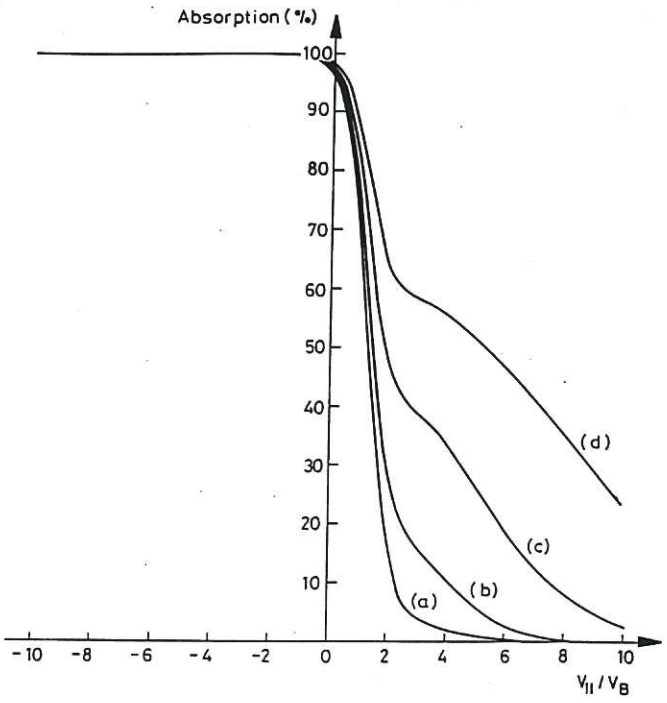

Fig. 4 Plasma parameters and launch angle the same as in Fig. 3. Tail parameters: $\mu=0.005$, $T_T=13.5\,keV$ and (a) $v_0=0.0$, (b) $v_0=1.5v_B$, (c) $v_B=3.0v_B$, (d) $v_0=4.5v_B$.

CLM-P755

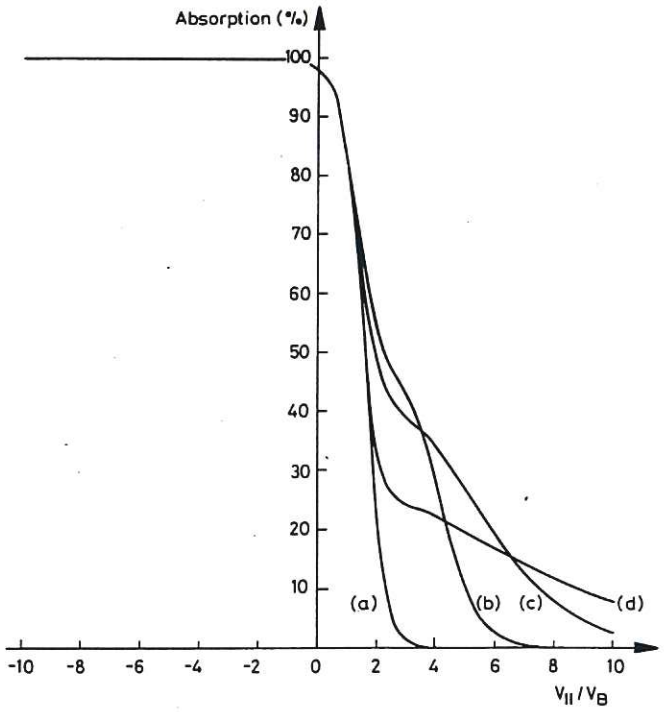

Fig. 5 Plasma parameters and launch angle the same as in Fig. 3. Tail parameters: $\mu=0.005$, $v_0=3.0v_B$ and (a) no tail, (b) $T_T=1.5$keV, (c) $T_T=13.5$ keV, (d) $T_T=150.0$ keV.

CLM-P755

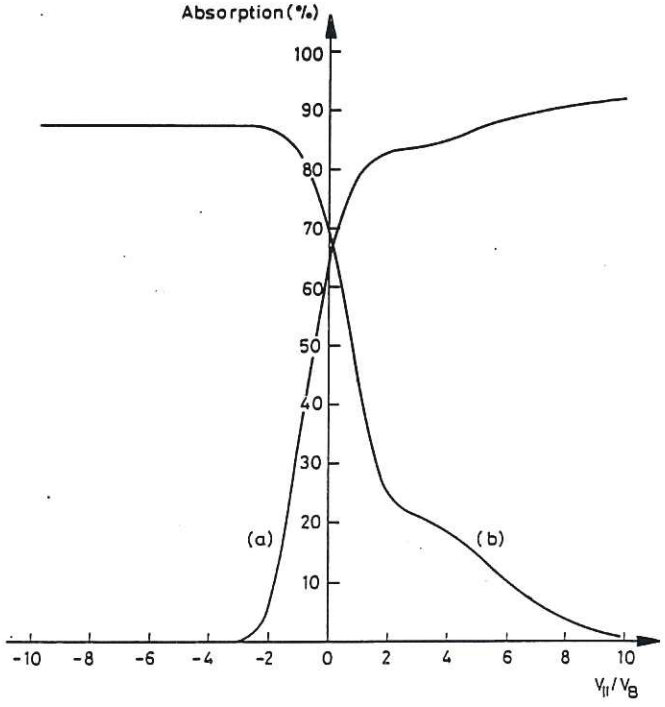

Fig. 6 Integrated power deposition profile for (a) $k_{\parallel} > 0$ ($\theta_0=60°$) and (b) $k_{\parallel} < 0$ ($\theta_0=120°$). $n_e(0)=6\times10^{19}\,m^{-3}$, $T_e(0)=1.5$ keV, $\mu=0.005$, $v_0=3.0v_B$, $T_T=13.5$ keV.

CLM-P755

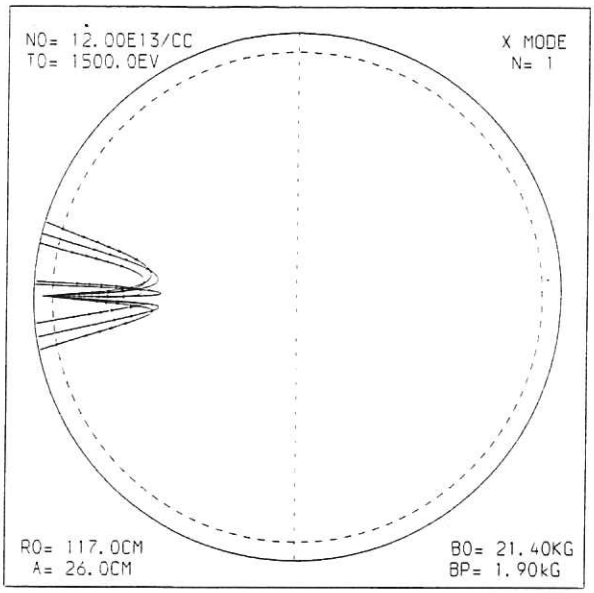

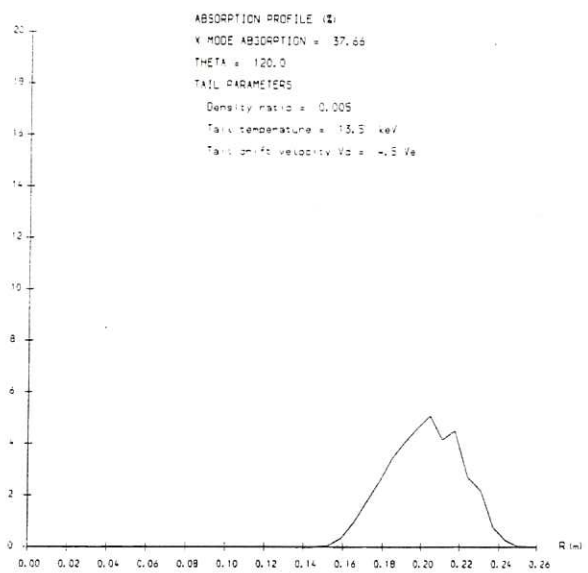

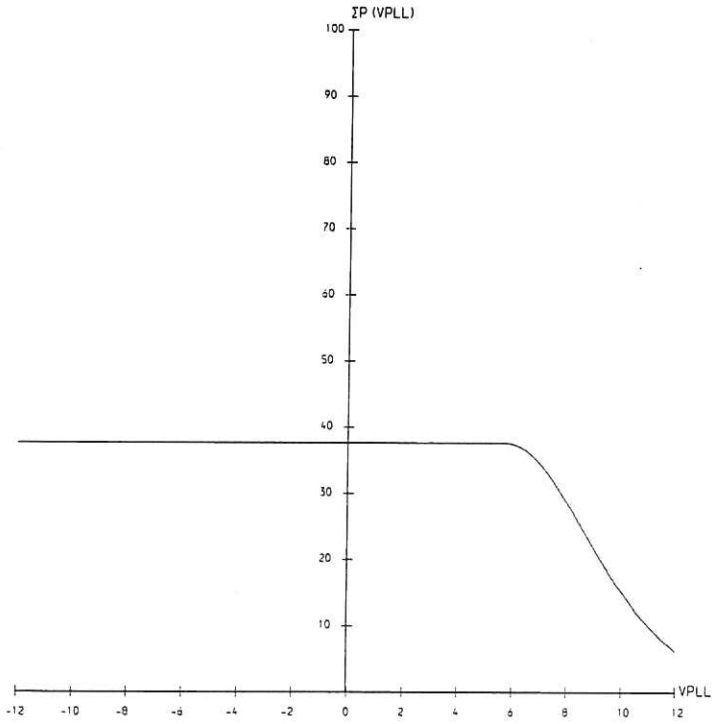

Fig. 7 (a) Minor cross section projection of ray trajectories in the presence of a tail for high-density plasma. The plasma parameters are displayed. (b) Power deposited per unit radial coordinate interval for the configuration of (a). (c) Integrated power deposition profile for the configuration of (a).

CLM-P755

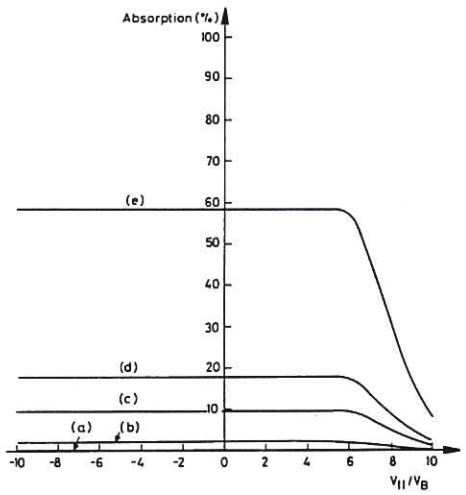

Fig. 8 Integrated power deposition profile. The rays are incident from the right. $n_e(0)=1.2\times10^{20}\,m^{-3}$, $T_e(0)=1.5\,keV$, launch angle 120°. Tail parameters: $v_0=3.0v_B$, $T_T=13.5\,keV$ and (a) $\mu=0.0$, (b) $\mu=0.001$, (c) $\mu=0.005$, (d) $\mu=0.001$, (e) $\mu=0.05$.

CLM-P755

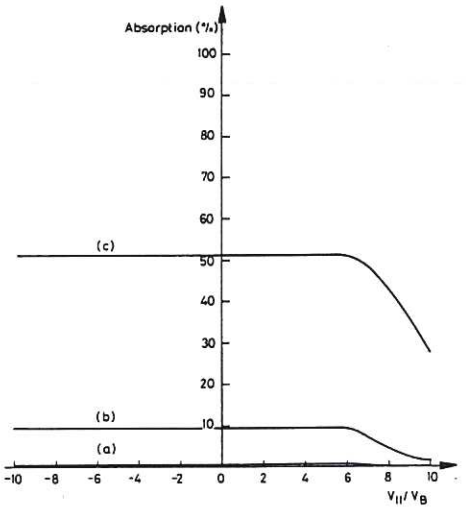

Fig. 9 Plasma parameters and launch angle the same as in Fig. 8 . Tail parameters: $\mu=0.005$, $T_T=13.5\,keV$, and (a) $v_0=v_B$, (b) $v_0=3.0v_B$, (c) $v_0=5.0v_B$.

CLM-P755

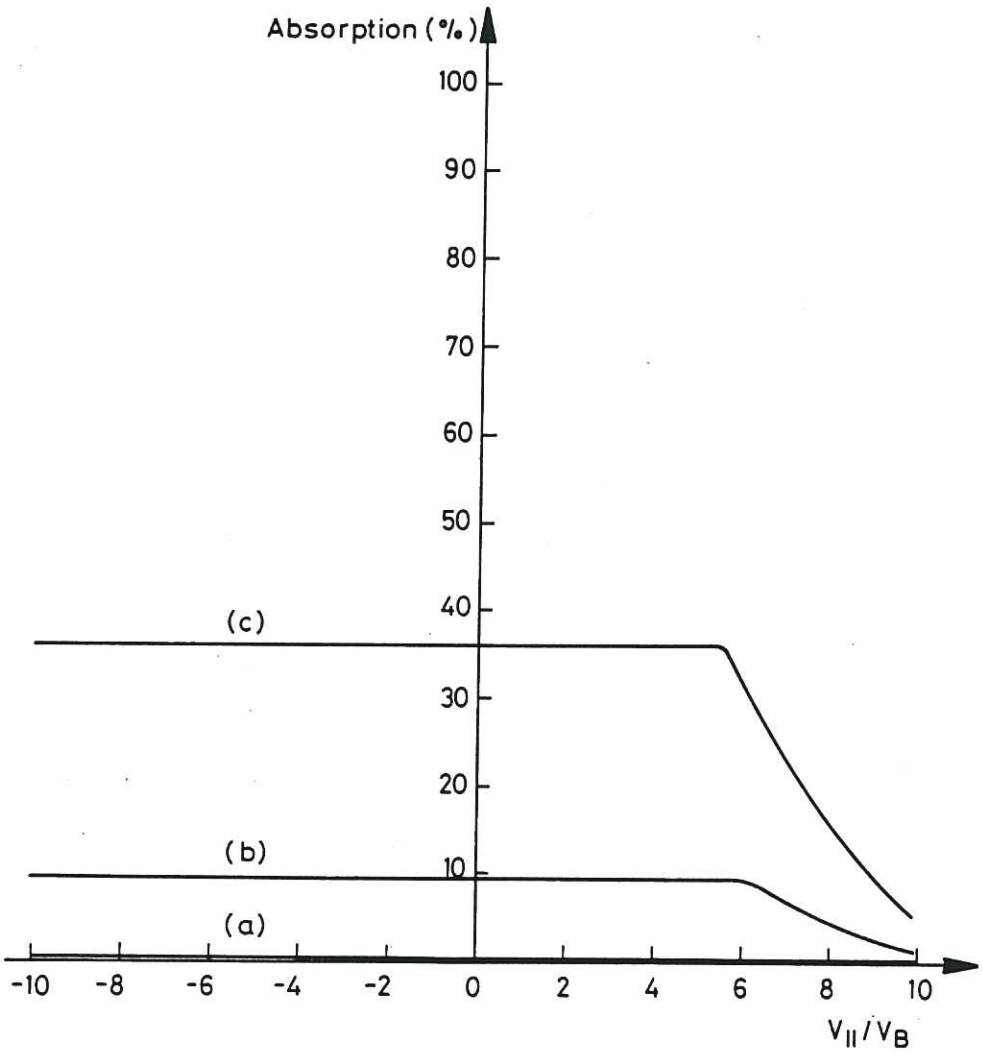

Fig. 10 Integrated power deposition profile, with launch angle as a parameter. Tail parameters $\mu=0.005$, $v_0=3.0\,b_B$, $T_T=13.5\,\text{keV}$. Plasma parameter $n_e(0)=1.2\times10^{20}\,\text{m}^{-3}$, $T_e(0)=1.5\,\text{keV}$, and launch angle is (a) 105°, (b) 120°, (c) 135°.

CLM-P755

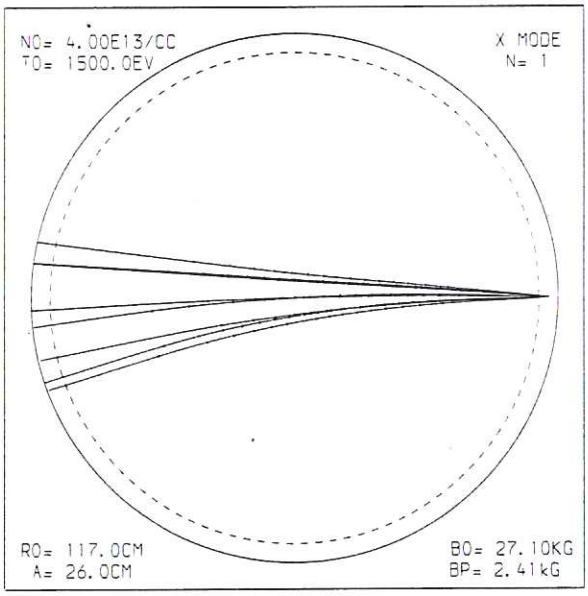

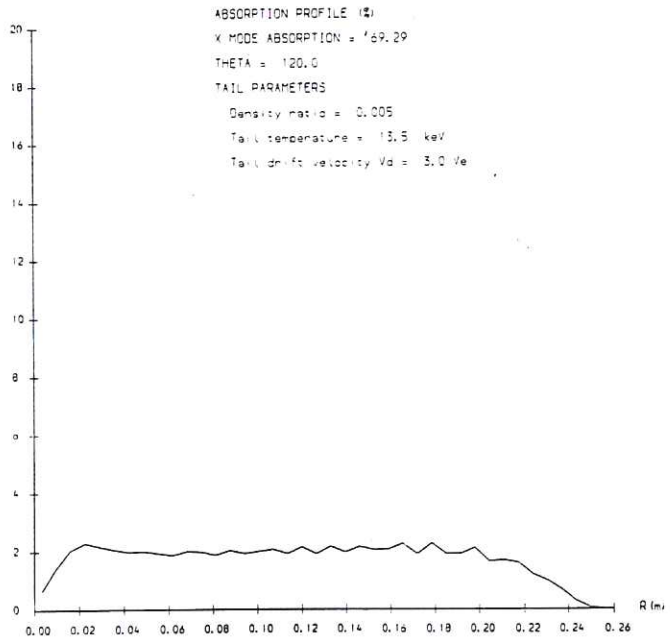

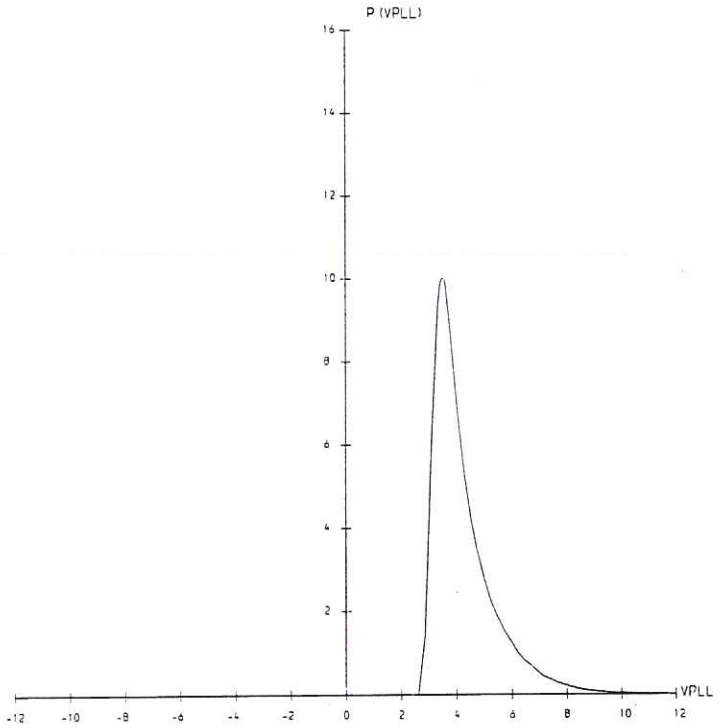

Fig. 11(a) Minor cross-section projection of ray trajectories in the presence of a tail for an X-mode launch position on the outside of the torus, with $\omega \ll \Omega_e$ (0) and the cyclotron resonance outside the torus. (b) Power deposited per unit radial coordinate interval for the configuration of 11(a). (c) Power deposition profile in velocity space. Parameter values are given in 11(a) and (b).

CLM-P755

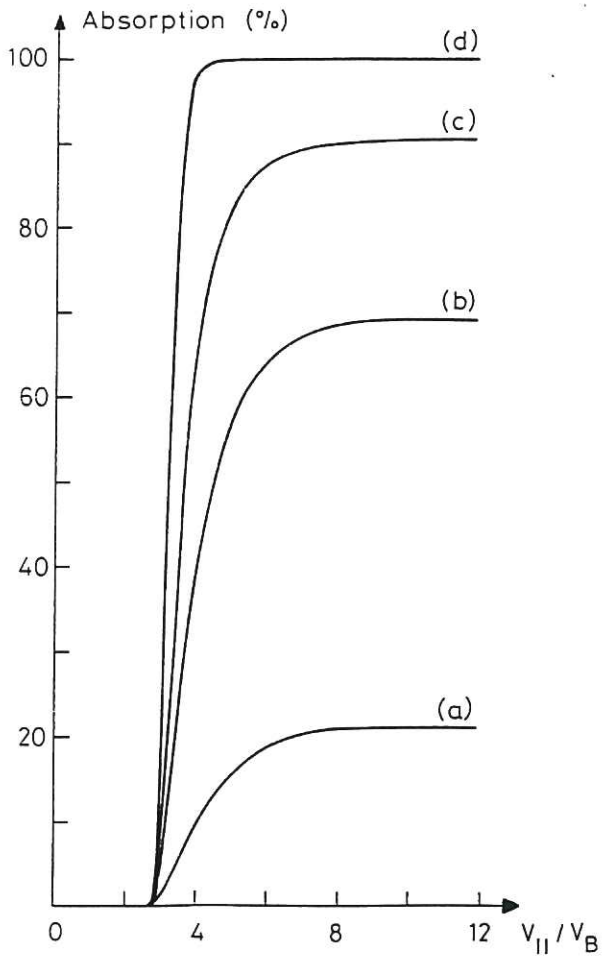

Fig. 12 Variation of absorption with tail density μ for the configuration of Figs.11(a),(b): (a) $\mu=0.005$, (b) $\mu=0.001$, (c) $\mu=0.01$, (d) $\mu=0.05$.

CLM-P755

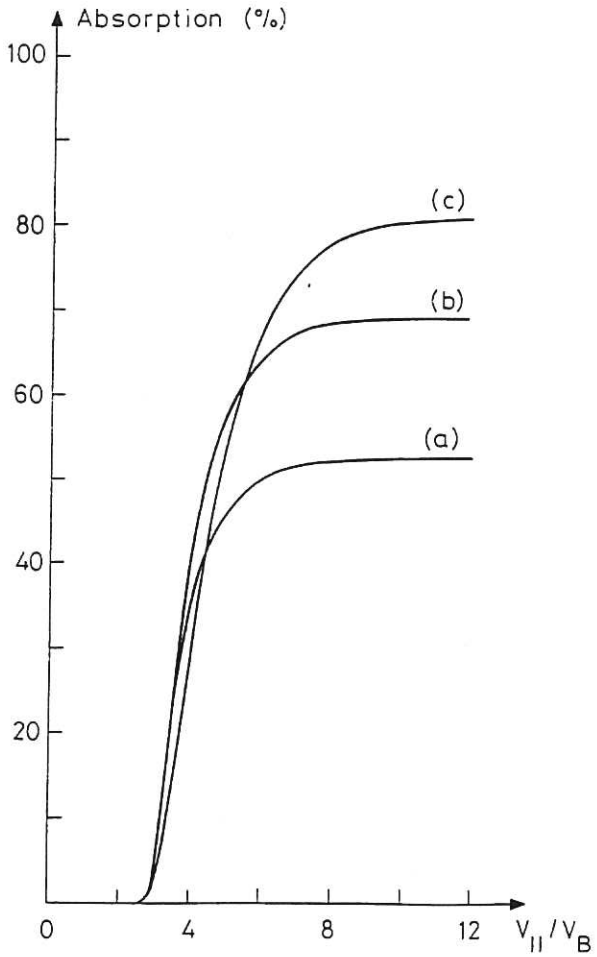

Fig. 13 Variation of absorption with tail drift velocity v_0 for configuration of Figs.11(a),(b): (a) $v_0=1.5V_B$, (b) $v_0=3.0v_B$, (c) $v_0=4.5v_B$.

CLM-P755

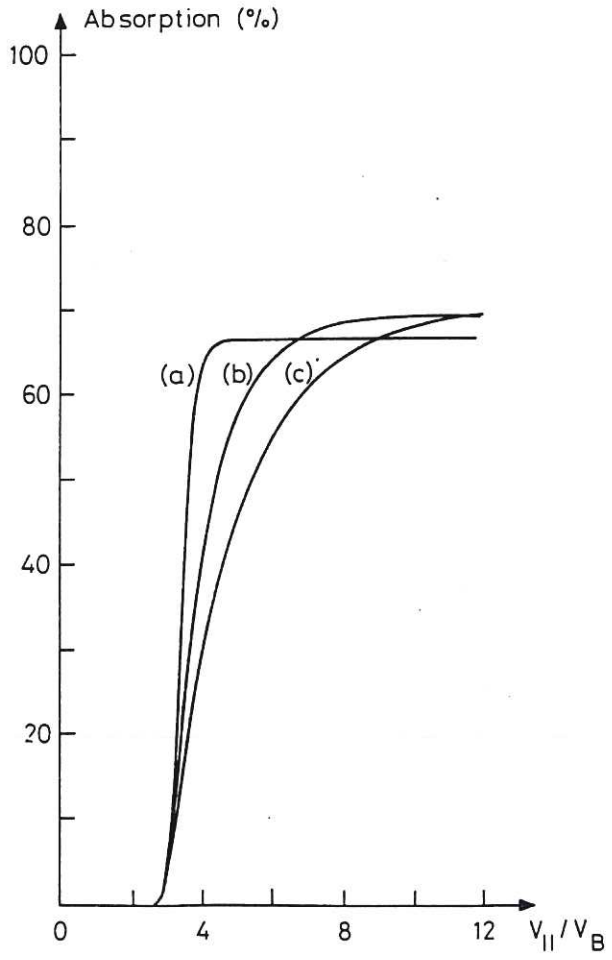

Fig. 14 Variation of absorption with tail thermal Velocity v_T for the configuration of Figs. 11(a), (b): (a) $v_T = 1.0 v_B$, (b) $v_T = 3.0 v_B$, (c) $v_T = 5.0 v_B$.

CLM-P755

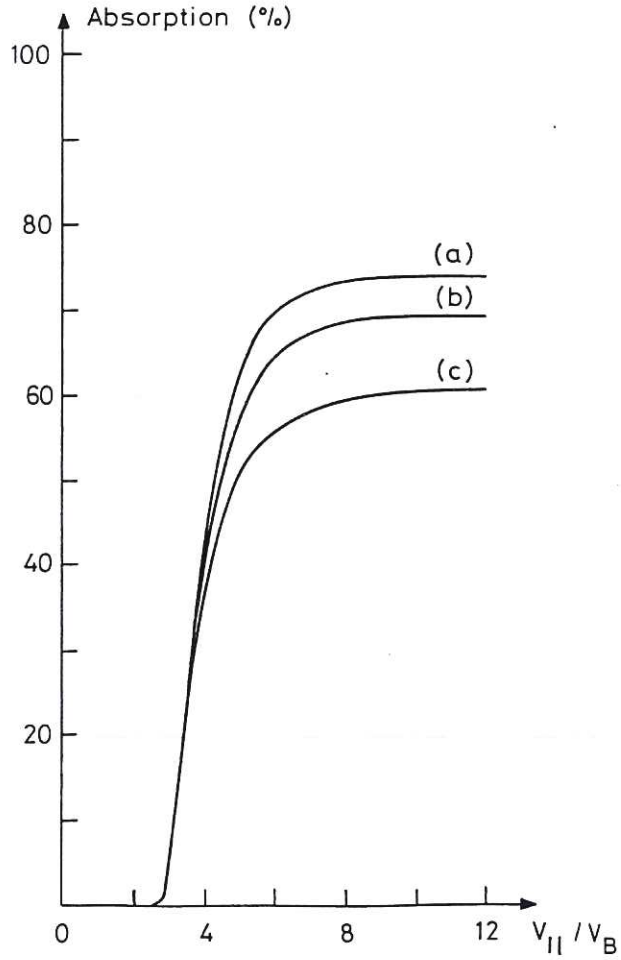

Fig. 15 Variation of absorption with bulk plasma density $n_e(0)$ for the configuration of Figs. 11(a),(b): (a) $n_e(0) = 2 \times 10^{19} \mathrm{m}^{-3}$, (b) $n_e(0) = 4 \times 10^{19} \mathrm{m}^{-3}$, (c) $n_e(0) = 6 \times 10^{19} \mathrm{m}^{-3}$.

CLM-P755